Extracting the kinetic parameters of the hydrogen evolution reaction at Pt in acidic media by means of dynamic multi-frequency analysis

Dominique Koster*[,a], Aleksandar R. Zeradjanin[b], Alberto Battistel[c], Fabio La Mantia*[,a]

[a] *Universität Bremen, Energiespeicher- und Energiewandlersysteme, Bibliothekstr. 1, 28359 Bremen, Germany*

[b]*Max Planck Institut für Eisenforschung, Interface Chemistry and Surface Engineering, Max Planck Strasse 1, 40237 Düsseldorf, Germany*

[c]*Department of Molecular Sciences and Nanosystems, University Cà Foscari Venice Via Torino, 155B, 30172 Mestre – Venezia, Italy*

Abstract

Herein, we use dynamic multi-frequency analysis (DMFA) to investigate the reaction kinetics of a paradigm electro-catalytic reaction, i.e. the hydrogen evolution reaction (HER) at polycrystalline Pt electrodes in acidic media. DMFA allows measuring dynamic impedance spectra under non-steady state conditions, as it is the case to avoid the formation of hydrogen bubbles. The extracted impedance spectra were fitted using electrical equivalent circuits (EECs) based on an analytical model, which took into account a Volmer-Tafel mechanism for hydrogen evolution. We found that the EECs based on this model can serve as suitable electrical analog in order to describe the physico-electrochemical processes that govern the different stages of the HER.

Keywords: dynamic impedance spectroscopy, dynamic multi-frequency analysis, electrolysis, hydrogen evolution reaction.

* Corresponding author: lamantia@uni-bremen.de (Fabio La Mantia)
koster@uni-bremen.de (Dominique Koster)

1. Introduction

The increasing energy demand and ongoing depletion of fossil fuels require the development of new technologies based on renewable and emission free sources that guarantee a reliable and inexpensive supply of energy [1]. In the frame of long-term energy storage, electro-catalysis plays an essential role in the production of valuable energy carriers, such as hydrogen [2]. In order to enable the future technologies, it is vital to understand what drives electro-catalytic reactions [3]. At this aim, the use of dynamic multi-frequency analysis (DMFA), which allows separating different phenomena in the total reaction mechanism with high temporal resolution and quantifying the kinetic parameters [4,5], becomes of fundamental importance.

Here we demonstrate the effectiveness of such methodology using the hydrogen evolution reaction (HER) on polycrystalline platinum as paradigm electro-catalytic reaction. Due to its high significance in various electrochemical applications, the HER has extensively been studied in acidic and basic media [6-10]. The reaction elementary steps involved in this process are well known, and the investigation of the underlying kinetics has been in the focus of various research contributions [11-14], although some points, such as the influence of the thermodynamics of adsorption on the exchange current density, are still matter of debate [15]. The HER involves three elementary reaction steps: Volmer, Tafel, and Heyrovsky. During the Volmer step the electrochemical adsorption of hydronium ions occurs, i.e. an H^+ is discharged at the electrode surface and an adsorbed H atom is formed. The latter acts as an intermediate in the HER process. Thereafter, the HER can proceed via two different pathways [16]. The first path is known as Tafel step and represents a purely chemical reaction of two adsorbed H-atoms under the formation of H_2, while the second path corresponds to the Heyrovsky step, where hydrogen

evolution occurs via an electron-transfer reaction [17]. The three elementary steps are here summarized:

$$M + H^+ + e^- \rightleftharpoons M - H \quad (1)$$

$$2M - H \rightleftharpoons 2M + H_2 \uparrow \quad (2)$$

$$M - H + H^+ + e^- \rightleftharpoons M + H_2 \quad (3)$$

Mechanistic studies of the HER process have mostly been performed by means of steady-state polarization methods, potential-step coulometry, potential relaxation techniques, and classical electrochemical impedance spectroscopy (EIS). Chialvo et al. studied the reaction kinetics of the HER and the HOR over the whole range of overpotentials by means of steady-state polarization at rotating disk electrodes, where the kinetic parameters were extracted from the current densities at different overpotentials [12,18], or by means of potentiodynamic sweep techniques [19]. However, as discussed recently, classic kinetics analysis at gas evolving electrodes using RDE can lead to wrong estimation of the mechanism and kinetic constants [20]. One of the problematic facts in the characterization of gas-evolving reactions is the influence of gas bubbles on the active surface area and consequently on obtaining accurate kinetic data. Namely, during the reaction the interfacial regions oversaturated with dissolved product do not contain sufficient amount of solvent, which should form a solvation sphere around each generated molecule. This leads to gas-bubble nucleation. Gas bubbles nucleate on the nanoscale, grow, and finally detach from the surface, thus periodically blocking a certain fraction of active sites. As consequence, the available (effective) surface area is somewhere between the geometric and real surface area. A usual misconception present in the literature is that gas bubbles can be removed with an imposed convective flow (e.g., by the application of RDE). However, from the Levich equation, even at 10000 rpm in aqueous electrolytes the size of diffusion layer is around 5 μm. This means that nanobubbles and even some microbubbles remain protected inside the diffusion layer, which

most authors overlook. To take into account this effect, it is necessary to develop methodologies for the correct estimation of the effective surface area, which is a routinely avoided challenge. While steady-state polarization methods might be useful in order to detect changes in the reaction kinetics, only EIS or potential relaxation techniques yield a quantitative analysis [13]. Characterization by means of Tafel parameters can help to identify the rate-determining electron-transfer reactions, however, one cannot unequivocally distinguish between contributions of different processes [21]. The activity of materials towards the HER is commonly interpreted by volcano-relationships, however, adsorption energies of H atoms cannot be attained experimentally; the results reported in literature often lead to contradictory interpretations [15]. Classical EIS gives an insight into reaction mechanisms and kinetic processes. However, the HER is an inner sphere reaction that involves the specific adsorption of H atoms on the electrode surface. Inner sphere reactions can only be investigated by classical EIS if the state of adsorption does not change within the time frame of the measurement, as this technique requires steady-state conditions. In contrast to other processes, e.g. the acetaldehyde oxidation at Pt, where steady-state conditions cannot even be attained after very long times [22], throughout the HER pseudo-steady state conditions might be readily achieved in potential regions where molecular hydrogen generation does not occur. This potential region was investigated by means of EIS in order to study the kinetics of hydrogen under potential deposition (HUPD) [14]. Similar studies were performed to investigate the effect of the surface lattice geometry on the (HUPD) kinetics [23]. In addition to that, EIS has been applied in order to characterize the hydrogen overpotential deposition (HOPD) on Pt single-crystal surfaces [13,24], where reliable impedance spectra could be recorded at low cathodic overpotentials. In contrast, when the measurements are carried out at high cathodic overpotentials, the impedance spectra are highly distorted over the whole frequency region because of the concomitant formation of hydrogen bubbles at the electrode. The higher is

the overpotential for the HER, the lower the quality of the spectra. Similarly, impedance spectra acquired during HER on Ni-Al electrodes showed poor quality at high overpotentials [16,25]. As the spectra appear distorted over the full range of frequencies, it is plausible that this effect is due to bubble nucleation, growth, coalescence and detachment, which occurs only if enough molecular hydrogen has been produce at the electrode's surface.

In this manuscript, we measured dynamic impedance spectra of the HER by means of DMFA, covering a large range of frequencies (from 1 MHz down to 8 Hz) at different concentrations of diluted perchloric acid (from 2 to 20 mM), thus investigating the possibility to identify the different elementary steps of the reaction mechanism, as well as the kinetic parameters and their quantification by means of an equivalent circuit based on the Volmer-Tafel mechanism. Due to the fast scan rate of the cyclic voltammetry (100 mV s^{-1}) and low concentration of hydronium, in our study we have no nucleation of hydrogen bubbles and good quality impedance data could be acquired and analyzed.

2. Experimental

Dynamic impedance spectra were recorded at RT in argon saturated solutions of 2, 5, 10, and 20 mM $HClO_4$ (Sigma-Aldrich). The measurements were performed in a cylindrical cell, equipped with a homemade Pt disk WE (Ø 250 µm), a Pt mesh CE (Labor Platina) and a Ag/AgCl/3M KCl RE [26]. The reference electrode was modified with a 100 µm-Pt wire and a parallel bypass 10 nF capacitor, in order to provide a constant voltage reference. Before each set of experiments, the WE was cleaned with abrasive paper (grade 12.6 µm, Matador) and manually polished with polishing paper of 3 and 1 µm grain size (3 M). Residual particles were removed by thoroughly rinsing the electrode with ultrapure water. Subsequently, the surface of the WE was electro-activated, by performing 100 voltammetric cycles in 100 mM $HClO_4$ in a potential

range between -0.25 V and 1.25 V vs. Ag/AgCl. No pre-electrolysis of the solutions was performed.

In order to perform DMFA measurements, the WE was polarized at a constant potential of 0.45 V vs. RHE, where the voltage signal was perturbed by a quasi-triangular wave which was superimposed by a multisinusoidal signal, created by a waveform generator using homemade Matlab scripts (release 2018a from the MathWorks Inc.). The current range of the potentiostat (VS-300, Bio-Logic) was set to 100 µA for 2 and 5 mM $HClO_4$, and to 1 mA for 10 and 20 mM $HClO_4$. The voltage input signal and the corresponding current response were detected by a 2-channel oscilloscope 4262 PicoScope (Pico technology). The quasi-triangular wave had amplitude of 1 V peak-to-peak and frequency of 50 mHz, thus corresponding to a scan rate of 100 mV/s. The multisine signal contained 45 frequencies covering 5 decades, where the base frequency was chosen to be 1 Hz, resulting in frequency values ranging from 1 MHz to 8 Hz (see supporting information, Appendix A, Figure S1). The amplitude of the multi-sine signal was 50 mV peak-to-peak. The amplitude was sufficiently low to guarantee an almost exclusive linear response of the system, as can be seen in the supporting information, Appendix B, Figure S5. In fact, the intermodulated signals, rising from the non-linearity of the frequency response, are 2 orders of magnitude smaller than the linear signals. In each measurement, a data point was recorded every 200 ns, where the total time of the experiment was 44 s, thus leading to 220 MSamples, from which 2000 impedance spectra were extracted. The data were evaluated by using homemade Matlab scripts. For more detailed information on design of the multi-sine perturbation and signal processing, the reader is referred to [5]. Data fitting was performed by complex non-linear regression, according to the procedure described in [4]. This is reported in the supporting information, Appendix C. Error estimation on the parameters was based on the covariance matrix weighted by the χ^2 value.

3. Results and Discussion

With the intent to investigate the possibility of extracting the kinetic parameters at low concentration of the electrolyte, despite of high ohmic resistance, we measured dynamic impedance spectra by means of DMFA during the HER on a polycrystalline platinum surface in contact with a perchloric acid solution at different concentrations, namely 2, 5, 10 and 20 mM. Keeping the potential sweeping avoids the formation of hydrogen bubbles and simplifies the interpretation of the results. Additionally, we intentionally avoided the use of supporting electrolyte, in order to decrease the interference of adsorbing anions (perchlorates are weakly adsorbing [27]) on the structure of the double layer [28] and consequently on the values of the measured kinetic parameters. Platinum activation cycle is reported in Appendix D, Figure S6. Here, double layer region and HUPD, with its characteristic peaks for polycrystalline platinum, are clearly visible.

Figure 1 shows the corresponding CVs recorded in a potential range between -0.55 V and +0.45 V vs. RHE at a scan rate of 100 mV s^{-1}. The shape of the voltammetry indicates a diffusion controlled reaction. To notice that at potentials more positive than 0 V (vs. RHE), hydronium adsorption through the Volmer step should occur, however this is not visible under the signal of hydrogen oxidation reaction (HOR), which is due to the hydrogen generated at potentials below 0 V (vs. RHE). At potentials between -0.13 and -0.22 V vs. RHE, the cathodic current density reaches a maximum and then declines, as expected for a diffusion controlled reaction. The maximum of the cathodic current densities is linearly growing with the concentration of the acid, thus indicating that the observed behavior is due to the diffusion limitation in solution. After the current peak, the rate of the HER is fully controlled by mass transport phenomena. By reversing the scan rate, once the potential is swept to values more positive than -50 mV vs. RHE, the

oxidation of the produced hydrogen, which still remains close to the platinum surface, becomes the governing process. At a potential of 0.03 V vs. RHE, an anodic current density peak is observed, where the electro-oxidation current increases with increasing electrolyte concentrations due to presence of the comparatively larger amounts of previously formed H_2.

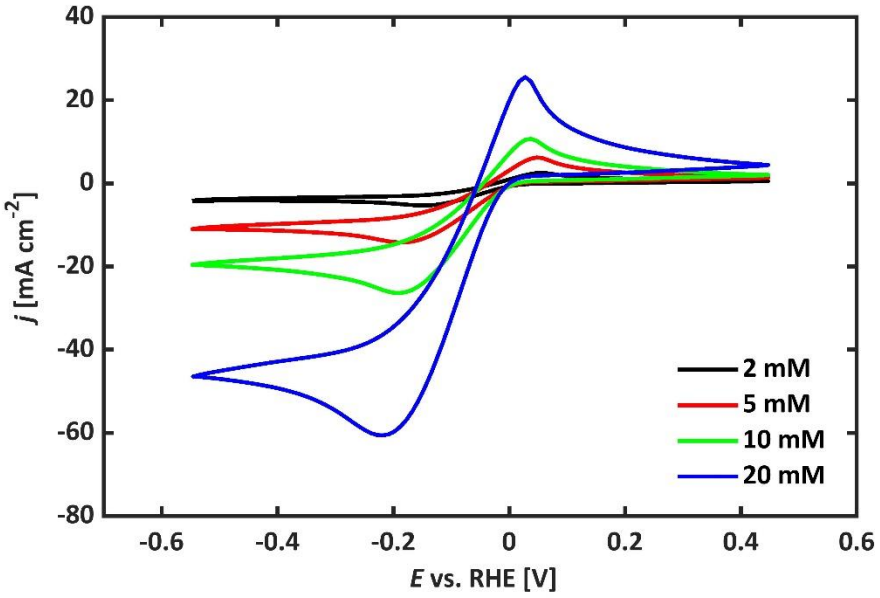

Figure 1: Cyclic voltammograms recorded at a scan rate of $\nu = 100$ mV s^{-1} in differently concentrated solutions of $HClO_4$.

The different stages of the HER were investigated by means of DMFA in the differently concentrated electrolyte solutions. A quasi-triangular potential perturbation was applied to the system, which was superimposed to a multi-sine wave, as described in the experimental. At first, we want to stress that the dynamic effects rising from the time-dependent diffusion profiles of molecular hydrogen and hydronium ions on the impedance spectra were clearly visible by confronting the impedance spectra acquired at the same potential during anodic and cathodic scans (see Supporting Information, appendix E, Figure S8).

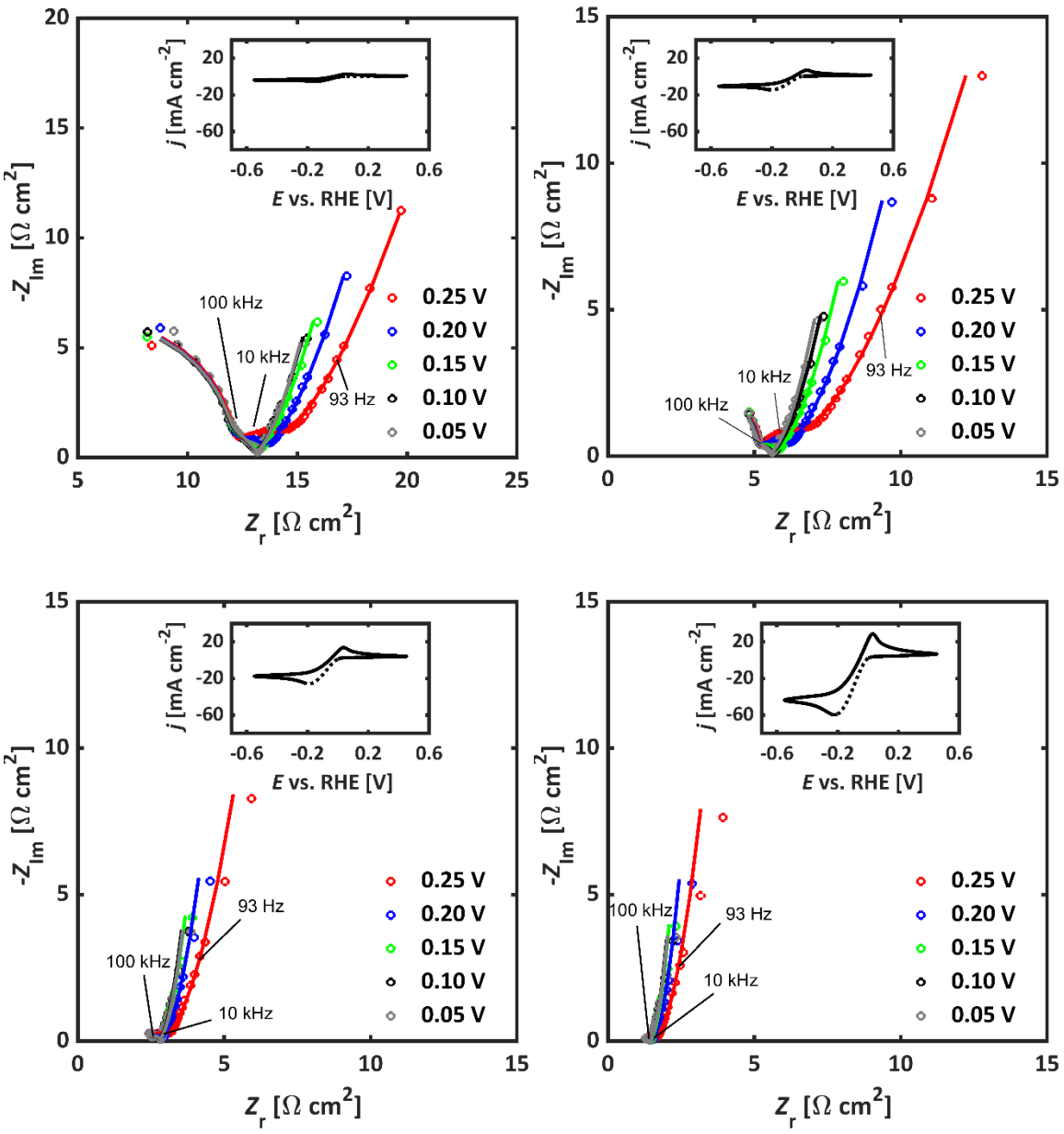

Figure 2: Dynamic impedance spectra recorded in differently concentrated solutions of $HClO_4$ (squares) and their corresponding fitted spectra (solid lines) at different potentials throughout the electrosorption region. (a) 2 mM $HClO_4$; (b) 5 mM $HClO_4$; (c) 10 mM $HClO_4$; (d) 20 mM $HClO_4$.

For sake of brevity and simplicity, we analyzed only the hydrogen electro-sorption and hydrogen evolution region during the cathodic scan. Figure 2 shows the experimental dynamic impedance spectra (dots) and their corresponding fitting (lines) in the different electrolyte solutions at

various potentials along the electro-sorption region. The potential range under investigation is governed by two competing processes, the discharge of hydronium ions at the electrode surface and the HOR, respectively.

The impedance spectra recorded for the different electrolyte solutions show a small semicircle at intermediate frequencies, which decreases in radius with higher electrolyte concentrations and when going towards more cathodic potentials. For this reason, the intermediate semicircle was attributed to the Volmer step (adsorption resistance). In the low frequency region, all the spectra show a straight line with a steep slope of around 67-86°, which we attributed to the diffusion-controlled adsorption of hydronium ions. The higher the concentration of the electrolyte and the more negative the potential, the steeper the slope, due to the lower influence of diffusion on the electro-sorption process. The high frequency region is governed by a fraction of a semicircle that cannot directly be related to a specific phenomenon. This feature becomes particularly dominant, when the electrolyte concentration is low and partially overlaps with the Volmer step. Graphical extrapolation of the curve in the high frequency region leads to an intercept with the real axis close to 0 Ω cm^2, which cannot be affiliated to the electrolyte resistance. Therefore we can attribute the high frequency semicircle to an artefact originating from the potentiostat input stray capacitance. In order to confirm this assumption, as well as to extract the kinetic parameters of the electro-sorption reaction, data fitting was performed under consideration of the parameter C_{st}, representing the stray capacitance of the potentiostat, as from Figure 3. With the help of an analytical model, based on the balance laws describing the chemico-physical properties of the processes of hydrogen evolution / oxidation, an equivalent circuit was constructed and used in the fitting routine. In the supporting information, Appendix F, we report the entire mathematical procedure. To notice that equation (F-24) of the supporting information is similar to the

expression obtained by B.E. Conway et al. in reference [24], equation (23). Figure 3a shows the graphical representation of equation (F-25) of the supporting information.

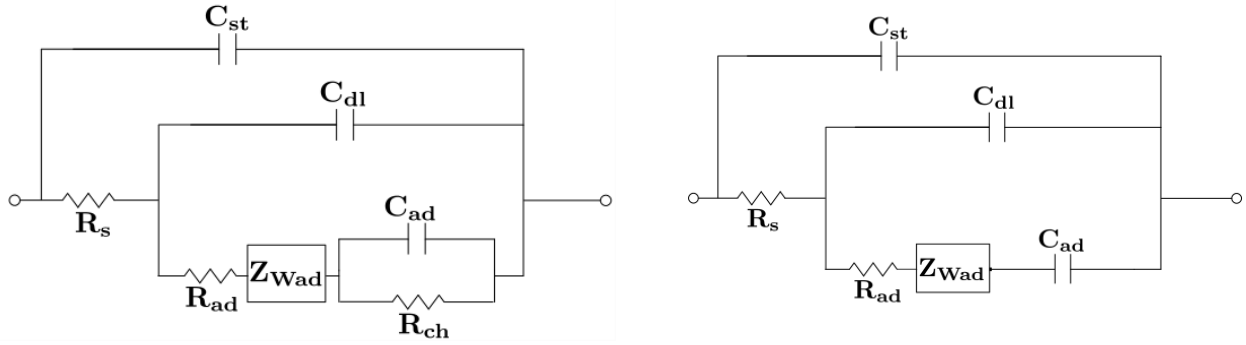

Figure 3: EECs constructed from an analytical model to fit the (a) hydrogen evolution region and the (b) electrosorption region.

The model was based on the assumption that H_2 generation exclusively follows the Volmer-Tafel mechanism. We want to stress that the Volmer-Heyrovsky mechanism does not lead to the same equivalent circuit in Figure 3a, as can be seen in Appendix G, where it is evident that the equation describing the Volmer-Heyrovsky mechanism is more complex and contains two more parameters. In order to distinguish between Volmer-Tafel and Volmer-Heyrovsky mechanism, it would be necessary to look at the dependence of the parameters on the potential. This is out of the scope of the present manuscript. The circuit elements represent the phenomena of adsorption and H_2 evolution, as well as diffusion processes, where R_s is referred to as the solution resistance, C_{dl} represents the charging of the double layer, R_{ad} is a measure of the limitation due to the faradaic process of electro-sorption, ZW_{ad} can be understood as the mass transport limitation of H^+ towards the surface, C_{ad} is related to the accumulation of adsorbed H, and R_{ch} is related to the recombination of two adsorbed hydrogen atoms. The physical meaning of the elements in terms of partial derivatives is given in Appendix F. While these parameters were allowed to move freely throughout the regression procedure, C_{st} was set to a constant value of 5 pF for all impedance spectra and all concentrations. We want to stress that, although the solution is quite

diluted and there is no supporting electrolyte, it is possible to describe migration and diffusion though the classic elements, R_s and σ, respectively, as reported in previous literature for redox couples [29].

Indeed, modeling revealed that this circuit gives an adequate physical representation of the reaction kinetics governing the processes of electro-adsorption and H_2 evolution in a potential range between -0.5 V and 0.05 V, while in the potential region where H_2 evolution does not yet occur (between 0.05 V and 0.45 V), R_{ch} attains infinitely high values and thus become physically meaningless. Fitting of the impedance spectra recorded in the electro-sorption region was therefore performed with the circuit shown in Figure 3b, which discards this parameter.

Figure 4 shows the kinetic parameters extracted from data fitting and their error bars for the different electrolyte concentrations as a function of potential. The error bars were obtained based on the formal covariance matrix of the χ^2 minimization. It is important to notice that, because we cannot make sure that the errors are normal-distributed in the DMFA measurements, these confidence intervals are only a rough estimation. The statistical analysis of the parameters is reported in the supporting information, Appendix H.

At 0.15 V vs. RHE, R_s values from 2.68 kΩ to 24.91 kΩ were extracted, where the solution resistance increased with decreasing electrolyte concentration. We want to stress that the error bars in the parameter R_s is always smaller than 1%. In the potential region under investigation the solution resistance remained practically constant. In order to confirm that these values are in a reasonable range, we calculated the theoretical specific resistance according to [30]

$$R_s = \frac{1}{4\kappa r}, \qquad (4)$$

where κ represents the ionic conductivity and r denotes the radius of the disk electrode (125 µm).

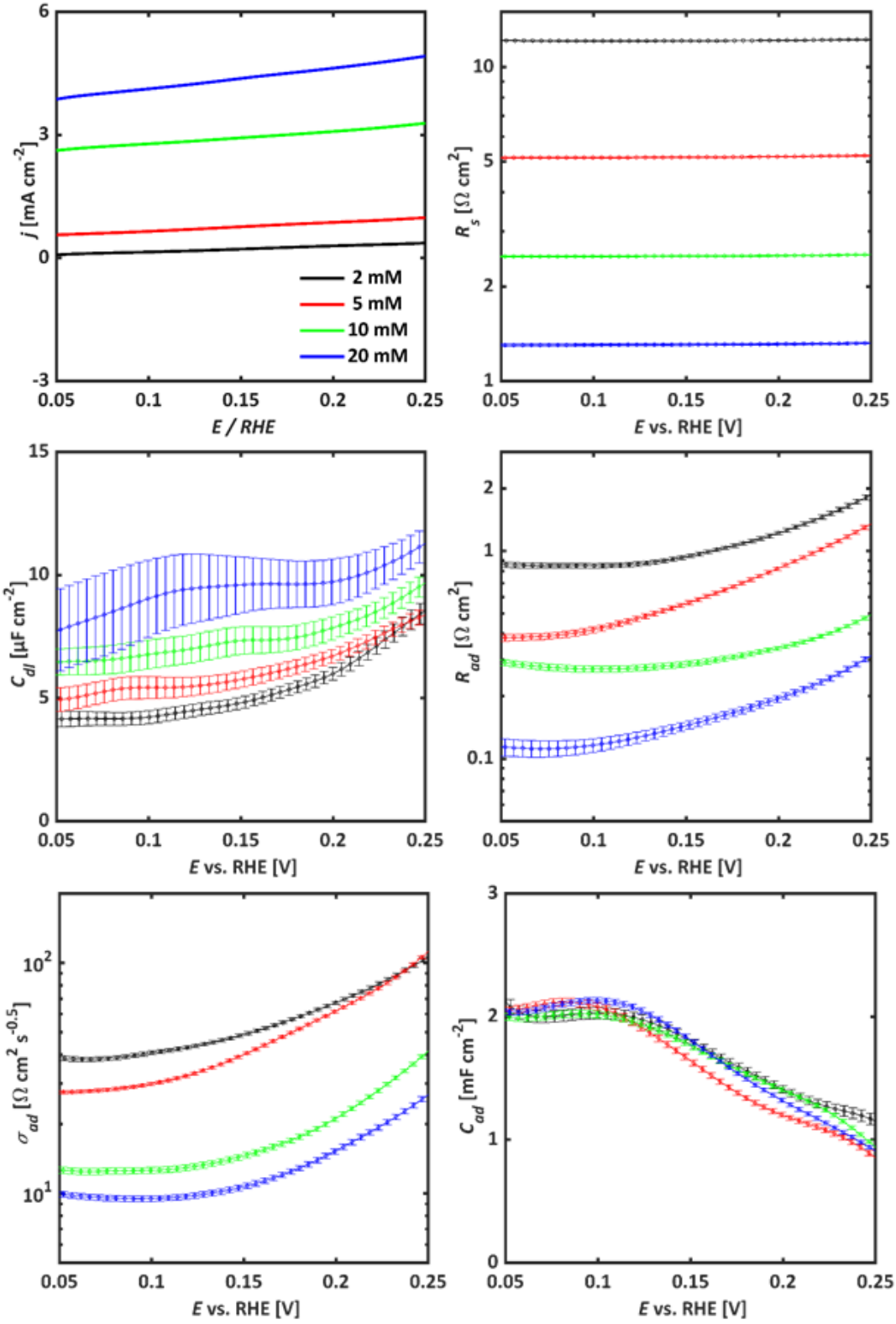

Figure 4: Variation of kinetic parameters extracted from data fitting of dynamic impedance spectra recorded in 2, 5, 10 and 20 mM $HClO_4$ in the electrosorption region.

Table 1 shows the solution resistances calculated for the different electrolytes, $R_{s\,cal}$, and the respective values extracted from data fitting, $R_{s\,fit}$, revealing that the calculated values match very well the fitting results. The potentiostat time constants, τ_{st}, were calculated from the values obtained for $R_{s\,fit}$ and C_{st} for the different electrolytes. In the same way, the adsorption time constants, τ_{ad}, were determined from R_{ad} and C_{dl}. The values of the time constants, as well as their corresponding characteristic frequencies, f_{st} and f_{ad}, are presented in Table 2. Although the characteristic frequencies related to the effect of the potentiostat lie above the maximum frequency applied throughout the measurements, it needs to be considered that smaller fractions of the characteristic values are still in a range where the potentiostat stray capacitance causes a significant distortion of the impedance signal. This means that the potentiostat can cause a distortion on the impedance spectra up to a frequency 10 times lower than f_{st}.

Table 1: Solution resistances calculated for a 250 µm Pt disk electrode in 2, 5, 10 and 20 mM $HClO_4$ and their corresponding values extracted from data fitting of dynamic impedance spectra recorded at 0.15 V vs. RHE.

c($HClO_4$) [mM]	**$R_{s\,cal}$ [Ω cm²]**	**$R_{s\,fit}$ [Ω cm²]**
2	11.8	12.1±0.08
5	4.71	5.15±0.03
10	2.35	2.51±0.02
20	1.17	1.31±0.01

The higher the electrolyte resistance, i. e. the lower the conductivity of the solution, the more dominant is the high frequency distortion, as the characteristic frequency related to this phenomenon shifts to ever lower values. While the spectrum recorded in 2 mM $HClO_4$ is highly distorted at all frequencies exceeding 26.80 kHz, in 20 mM $HClO_4$, the influence of the stray capacitance cannot be neglected only at frequency values higher than 267.40 kHz. For the

respective concentrations, the time constants related to the electro-sorption reaction considerably differ from those corresponding to stray capacitance effects, where the ratio between τ_{st} and τ_{ad} increases with increasing electrolyte concentration.

Table 2: Time constants and characteristic frequencies related to the processes governing the adsorption region calculated from the kinetic parameters extracted from data fitting of dynamic impedance spectra recorded at 0.15 V vs. RHE.

c($HClO_4$) [mM]	**τ_{st} [ns]**	**f_{st} [MHz]**	**τ_{ad} [µs]**	**f_{ad} [kHz]**
2	120	1.30	4.10	39.0
5	53.0	3.00	3.10	51.0
10	26.0	6.20	2.20	74.0
20	13.0	12.0	1.30	120

The adsorption resistance, R_{ad}, is in anti-symmetry with respect to C_{ad} where the kinetic limitation slightly decreases, when going towards cathodic potentials until a minimum is reached at around 0.15 V vs. RHE. Then R_{ad} slowly increases again, as the surface coverage of atomic H increases and mass transport of reactive species to the electrode surface decreases. The Warburg coefficient, σ_{ad}, follows the same trend as R_{ad}. Within the error bars of the fitting, it is clear that C_{ad} is a weak function of the H^+ concentration, while R_{ad} and σ_{ad} strongly depend on it, as expected.

Figure 5 shows the measured (dots) and fitted (lines) impedance spectra in the differently concentrated electrolyte solutions in a potential range between -0.2 and 0 V vs. RHE (cathodic scan direction), where H_2 evolution occurs. Although the overall impedance decreases with increasing electrolyte concentration, due to an increase in ionic conductivity, the impedance spectra follow the same trends along the potential scale under investigation.

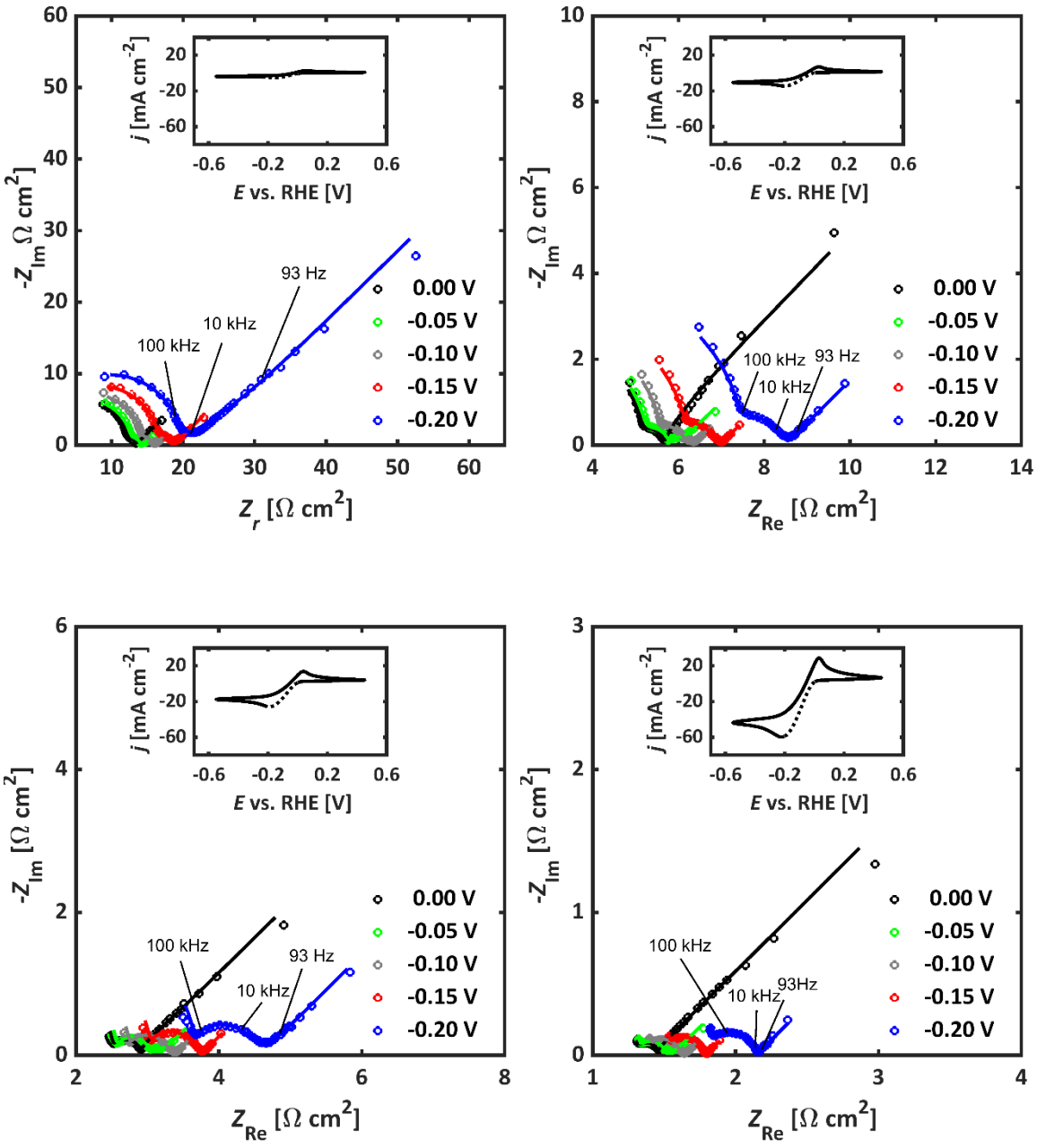

Figure 5: Dynamic impedance spectra recorded in differently concentrated solutions of $HClO_4$ (circles) and their corresponding fitted spectra (lines) at different potentials in the HER region. (a) 2 mM $HClO_4$; (b) 5 mM $HClO_4$; (c) 10 mM $HClO_4$; (d) 20 mM $HClO_4$.

Similarly to the results presented in Figure 2, the high frequency region is dominated by the artefact due to the potentiostat stray capacitance. The artefact partially (5-20 mM $HClO_4$) or fully

(2 mM $HClO_4$) covers the features related to the processes of electro-sorption and hydrogen generation, which appear as a slightly distorted single semicircle at intermediate frequencies. With decreasing potentials, the spectra are shifted towards more positive values along the x-axis, which might be attributed to an increase in the resistance values, R_s, R_{ad}, and R_{ch}, in the course of the HER. Differently to what was observed in the adsorption region, the radius of the distorted semicircle increases with increasing overpotential. In addition to that, at low frequencies the curve evolves into a straight line having a slope of 45°, which is clearly related to a diffusion process. Data fitting was performed with the EEC shown in Figure 3a, where the regression of the model to the experimental data resulted in values of χ^2 below $3 \cdot 10^{-5}$.

Table 3: Time constants and characteristic frequencies related to the processes governing the HER region calculated from the kinetic parameters extracted from data fitting of dynamic impedance spectra recorded at -0.1 V vs. RHE.

c($HClO_4$) [mM]	**τ_{ad} [µs]**	**f_{ad} [kHz]**	**τ_{ch} [µs]**	**f_{ch} [kHz]**
2	5.30	30.0	50.0	2.88
5	2.70	60.0	40.0	3.59
10	3.70	43.0	30.0	4.36
20	1.70	93.0	18.8	8.45

Figure 6 shows the variation of the extracted kinetic parameters and their error bars within the potential range under investigation. It is interesting to observe that R_{ad} increases when moving towards negative potentials, indicating that the kinetics of the electro-sorption process become more sluggish, due to the local decrease in concentration of the hydronium ions. This is observed also in redox couples [5].

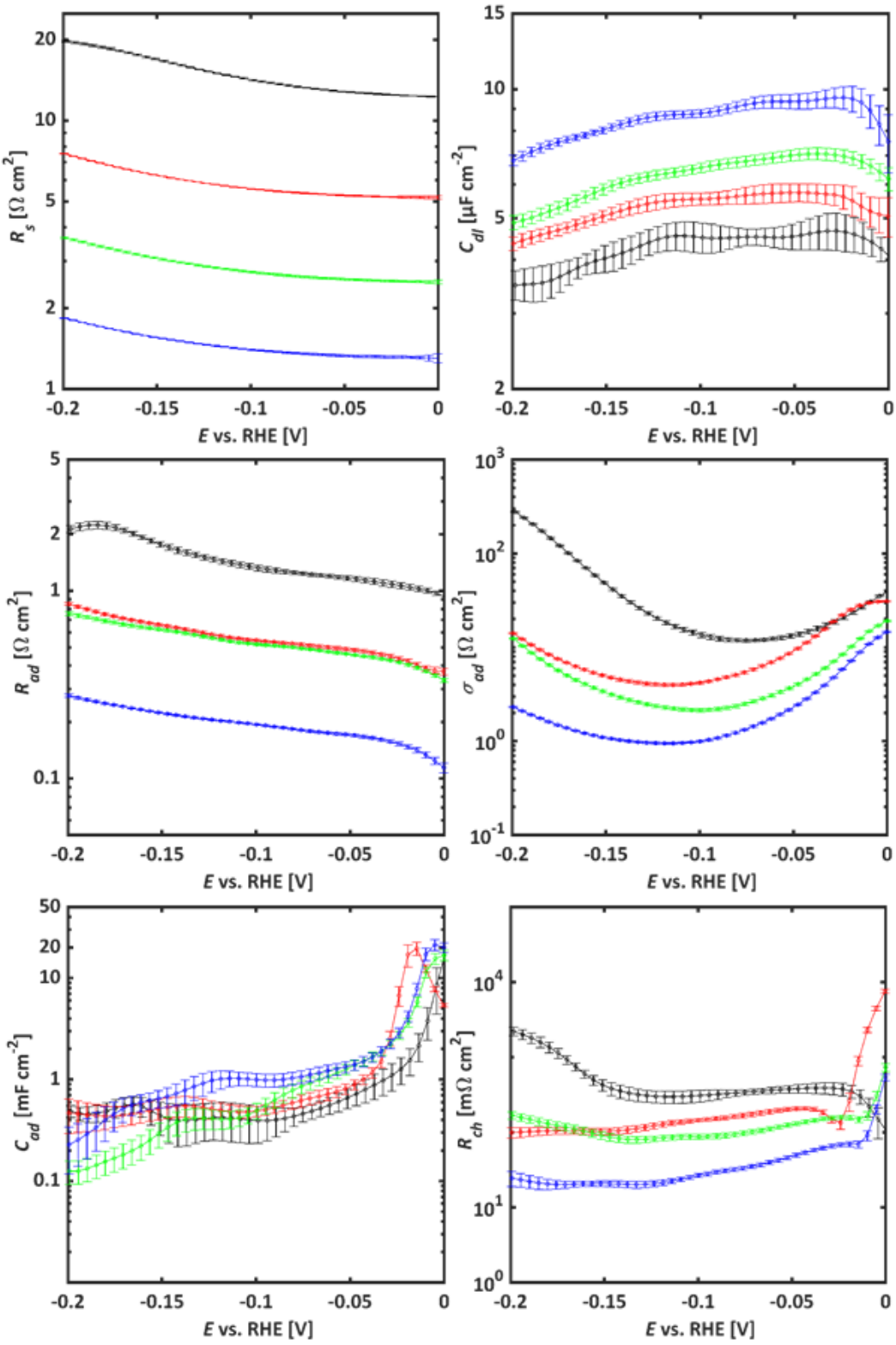

Figure 6: Variation of kinetic parameters extracted from data fitting of dynamic impedance spectra recorded in 2, 5, 10 and 20 mM $HClO_4$ in the HER region.

This is further supported by the fact that R_s increases at cathodic potentials, due to the ever lower amount of acid close to the surface of the electrode. The lower is the initial electrolyte concentration, the faster the depletion of the reactant. τ_{ad} and f_{ad} are in a similar range as the values reported in Table 2, and follow a similar trend, while f_{ch} is only one order of magnitude lower than f_{ad} in all cases. This fact, in addition to the slightly smaller value of R_{ch} with respect to R_{ad} makes very difficult to optically distinguish the two semicircles of the two steps in the Nyquist plots acquired in this potential range. In fact, here Volmer step and Tafel step have comparable rates, contrary to the expectation that Tafel step is rate determining for the HER on Pt in acidic media. This indicates that concentration of hydronium ions can influence the reaction pathway. Also because of the narrow range of frequencies in which C_{ad} is observable, its error is much larger than that of the other parameters. However, it is clear that C_{ad} is decreasing with the potential and is weakly dependent on the concentration of hydronium ions. Striking feature of Cad is its sudden change in proximity of the reversible hydrogen potential, which spans almost one order of magnitude. This phenomenon is very intriguing and indicates some drastic changes in the structure of the adsorbates and double layer. The parameter σ_{ad} has a very small error bar and shows a clear minimum, which corresponds to the potential at which the current density has the largest slope (see Figure 1). R_{ch} seems to reach a minimum at potentials around -0.15 V vs. RHE, and finally remains constant or increases slowly when the potential is swept towards negative potentials. The statistical significance of all the parameters is reported in the section H of the supporting information. Running the t-test for all parameters and also for the complete equivalent circuit (equation (F-24) in supporting information) shows that equivalent circuits with larger number of parameters were not necessary; however it does not indicate that this is the correct mechanism.

We want to stress again that R_{ad} and R_{ch} do not decrease with an exponential law, as expected from the classic Butler-Volmer equation, due to the effect of diffusion of reactant and products on the kinetics. This is a very well-known behavior (see for example reference [5]). The behavior of these parameters can be again interpreted in terms of a growing H^+ depletion layer in front of the electrode surface. Since R_{ad} is only slightly larger than R_{ch}, the electro-sorption reaction represents the rate determining step in the mechanism of reaction, at variance with reports in literature [13]. However, we want to stress that the most striking characteristics of these measurements is that, under the given experimental conditions, despite the low concentration pof electrolyte and the absence of supporting electrolyte, which makes the resistance of the solution, $R_{s,}$, dominating the kinetics of the HER, it is possible to extract the resistances related to the mechanism itself. This opens the way to analyze HER and HOR under experimental conditions, where interference of anions originating from main or supporting electrolyte is minimized. This could be of high importance for further mechanistic studies.

4. Conclusion

The reaction kinetics of the HER has been studied in diluted acidic media at Pt electrodes by means of DMFA, where dynamic impedance spectra were recorded at each point of a voltammetric scan. In the high frequency region the Nyquist plots were distorted by potentiostat stray capacitance effects, which became particularly dominant when the concentration of the electrolyte was very low. Therefore, the stray capacitance was included in the fitting procedure. EECs constructed from an analytical model based on the Volmer-Tafel mechanism gave an adequate physical description of the different processes governing the underpotential deposition of H as well as HER. It is important to stress, that this methodology enables the extraction of reliable kinetic parameters, despite high ohmic resistance of main electrolyte and absence of

supporting electrolyte. The extracted parameters are showing similar dependence on the potential, independently from the electrolyte concentration. Particularly interesting features were: 1) Volmer and Tafel step have comparable rates in diluted electrolytes, opposite to usual perception that HER on Pt in acidic media is controlled by Tafel step; 2) C_{ad} exhibits drastic change in proximity of reversible potential for HER, which indicates some unknown reconstruction of the interfacial region. This will be the focus of coming studies.

Acknowledgement

This project has received funding from the European Research Council (ERC) under the European Union's Horizon 2020 research and innovation programme (grant agreement n° 772579).

References

[1] K. Bennaceur, B. Clark, F.M. Orr, Jr., T.S. Ramakrishnan, C. Roulet, E. Stout., Hydrogen: A Future Energy Carrier?, Oilfield Review. 17(1) (2005) 30-41.
[2] I. Dincer., Green Methods for Hydrogen Production, International Journal of Hydrogen Engergy. 37 (2012) 1954-1971.
[3] D.M.F. Santos, C.A.C. Sequeira, J.L. Figueiredo, Hydrogen Production by Alkaline Water Electrolysis. Quimica Nova 36 (2013) 1176-1193
[4] A. Battistel, G. Du, F. La Mantia, On the Analysis of Non-stationary Impedance Spectra Electroanalysis. 28 (2016) 2346-2353.
[5] D. Koster, G. Du, G., A. Battistel, F. La Mantia, Dynamic Impedance Spectroscopy Using Dynamic Multi-Frequency Analysis: A Theoretical and Experimental Investigation, Electrochim. Acta. 246 (2017) 553-563.
[6] B.E. Conway, J.O'M Bockris, Electrolytic Hydrogen Evolution Kinetics and its Relation to the Electronic and Adsorptive Properties of the Metal. The Journal of Chemical Physics. 26 (1957) 532-541.
[7] S. Trasatti, Work Function, Electronegativity, and Electrochemical Behaviour of Metals. III. Electrolytic Hydrogen Evolution in Acid Solutions. Electroanalytical Chemistry and Interfacial Electrochemistry. 39 (1972) 163-184.
[8] G. Jerkiewicz, Hydrogen Sorption at/in Electrodes. Progress in Surface Science. 57 (1998) 137-186.

[9] F.P Bowden, E.K. Rideal, The Electrolytic Behaviour of Thin Films. Part I. Hydrogen. Proceedings of the Royal Society A, Mathematical, Physical and Engineering Science. 120 (1928) 59-79.
[10] A. Lasia, 2003. Handbook of Fuel Cells - Fundamentals, Technology and Applications, Volume 2: Electroctalysis. John Wiley & Sons, New Jersey.
[11] M.D. Arce, H.L. Bonazza, J.L. Fernandez, Kinetic Analysis of the Hydrogen Evolution Reaction in Unbuffered Media. Theory and Studies on Pt Microelectrodes. Electrochimica Acta, 107 (2013) 248-260.
[12] P.M. Quaino, M.R. Gennero de Chialvo, A.C. Chialvo, Hydrogen Evolution Reaction: A Complete Kinetic Description. Electrochimica Acta. 52 (2007) 7396-7403.
[13] J. Barber, S. Morin, S., B.E. Conway, Specificity of the Kinetics of H_2 Evolution to the Structure of Single-crystal Pt Surfaces, and the Relation between OPD and UPD H. Journal of Electroanalytical Chemistry. 446 (1998) 125-138.
[14] B. Losiewicz, R. Jurczakowski, A. Lasia, Kinetics of the Hydrogen Underpotential Deposition at Polychristalline Platinum in Acidic Solutions. Electrochimica Acta. 80 (2012) 292-301.
[15] A.R Zeradjanin, J.P. Grote, G. Polymeros, K.J.J. Mayrhofer, A Critical Review on Hydrogen Evolution Electrocatalysis: Re-exploring the Volcano-relationship. Electroanalysis. 28 (2016) 2256-2269.
[16] L. Birry, A. Lasia, Studies of the Hydrogen Evolution Reaction on Raney-Nickel-Molybdenum. Journal of Applied Electrochemistry. 34 (2004) 735-749.
[17] B.E. Conway, B.V. Tilak, Interfacial Processes Involving Electrocatalytic Evolution and Oxidation of H_2, and the Role of Chemisorbed H. Electrochimica Acta. 47 (2002) 3571-3594.
[18] M.S. Rau, M.R. Gennero de Chialvo, A.C. Chialvo, Kinetic Study of the Hydrogen Oxidation Reaction on Pt over the Complete Potential Range. Journal of Power Sources. 229 (2013) 210-215.
[19] C.A. Marozzi, M.R. Gennero de Chialvo, A.C. Chialvo, Criteria for the Selection of the Scan Rate in the Evaluation of the Kinetic Paramters of the Hydrogen Oxidation Reaction by a Potentiodynamic Sweep. Journal of Electroanalytical Chemistry. 748 (2015) 61-69.
[20] A.R Zeradjanin, Frequent Pitfalls in the Characterization of Electrodes Designed for Electrochemical Energy Conversion and Storage. ChemSusChem. 11 (2018) 1278-1284.
[21] H. Vrubel, T. Moehl, M. Grätzel, X Hu, Revealing and Accelerating Slow Electron Transport in Amorphous Molybdenum Sulphide Particles for Hydrogen Evolution Reaction. Chemical Communications. 49 (2013) 8985-8987.
[22] C. Desilets, A. Lasia, Dynamic Impedance Study of Ethanol and Acetaldehyde Oxidation at Platinum in Acid Solutions. Electrochimica Acta. 78 (2012) 286-293.
[23] S. Morin, S., H. Dumont, B.E. Conway, Evaluation of the Effect of Two-Dimensional Geometry of Pt Single-Crystal Faces on the Kinetics of UPD of H Using Impedance Spectroscopy. Journal of Electroanalytical Chemistry. 412 (1996) 39-52.
[24] B.E. Conway, J. Barber, S. Morin, Comparative Evaluation of Surface Structure Specificity of Kinetics of UPD and OPD of H at Single-Crystal Pt Electrodes. Journal of Electroanalytical Chemistry. 44 (1998) 1109-1125.
[25] P. Los, A. Rami, A. Lasia, Hydrogen Evolution Reaction on Ni-Al Electrodes. Journal of Applied Electrochemistry. 23 (1993) 135-140.

[26] A. Battistel, M. Fan, J. Stojadinović, F. La Mantia, Analysis and Mitigation of the Artefacts in Electrochemical Impedance Spectroscopy due to Three-Electrode Geometry. Electrochim. Acta 135 (2014) 133-138.
[27] J. Omura, H. Yano, D. A. Tryk, M. Watanabe, H. Uchida, Electrochemical Quartz Crystal Microbalance Analysis of the Oxygen Reduction Reaction on Pt Based Electrodes. Part 2: Adsorption of Oxygen Species and ClO_4^- Anions on Pt and Pt-Co Alloy in $HClO_4$ Solutions, American Chemical Society, 30 (2014) 432-439.
[28] A. R Zeradjanin, A. A. Vimalanandan, G. Polymeros, A. A. Topalov, K. J. J. Mayrhofer, M. Rohwerder, Balance Work Function as a Driver for Facile Hydrogen Evolution Reaction – Comprehension and Experimental Assessment of Interfacial Catalytic Descriptor, Phys.Chem.Chem.Phys 19 (2017) 17019-17027.
[29] G. Du, F. La Mantia, Coupling the Charging Current and the Electron Transfer Process: the Effect on Impedance Spectra, ChemElectroChem 4 (2017) 122-129.
[30] M.E. Orazem, B. Tribollet, Electrochemical Impedance Spectroscopy, 1st ed., John Wiley & Sons, New Jersey, 2008.

Figure and Table captions

Figure 1: Cyclic voltammograms recorded at a scan rate of ν = 100 mV s^{-1} in differently concentrated solutions of $HClO_4$.

Figure 2: Dynamic impedance spectra recorded in differently concentrated solutions of $HClO_4$ (squares) and their corresponding fitted spectra (solid lines) at different potentials throughout the electrosorption region. (a) 2 mM $HClO_4$; (b) 5 mM $HClO_4$; (c) 10 mM $HClO_4$; (d) 20 mM $HClO_4$.

Figure 3: EECs constructed from an analytical model to fit the (a) hydrogen evolution region and the (b) electrosorption region.

Figure 4: Variation of kinetic parameters extracted from data fitting of dynamic impedance spectra recorded in 2, 5, 10 and 20 mM $HClO_4$ in the electrosorption region.

Figure 5: Dynamic impedance spectra recorded in differently concentrated solutions of $HClO_4$ (squares) and their corresponding fitted spectra (solid lines) at different potentials in the HER region. (a) 2 mM $HClO_4$; (b) 5 mM $HClO_4$; (c) 10 mM $HClO_4$; (d) 20 mM $HClO_4$.

Figure 6: Variation of kinetic parameters extracted from data fitting of dynamic impedance spectra recorded in 2, 5, 10 and 20 mM $HClO_4$ in the HER region.

Table 1: Solution resistances calculated for a 250 μm Pt disk electrode in 2, 5, 10 and 20 mM $HClO_4$ and their corresponding values extracted from data fitting of dynamic impedance spectra recorded at 0.15 V vs. RHE.

Table 2: Time constants and characteristic frequencies related to the processes governing the adsorption region calculated from the kinetic parameters extracted from data fitting of dynamic impedance spectra recorded at 0.15 V vs. RHE.

Table 3: Time constants and characteristic frequencies related to the processes governing the HER region calculated from the kinetic parameters extracted from data fitting of dynamic impedance spectra recorded at -0.1 V vs. RHE.

Figure 1

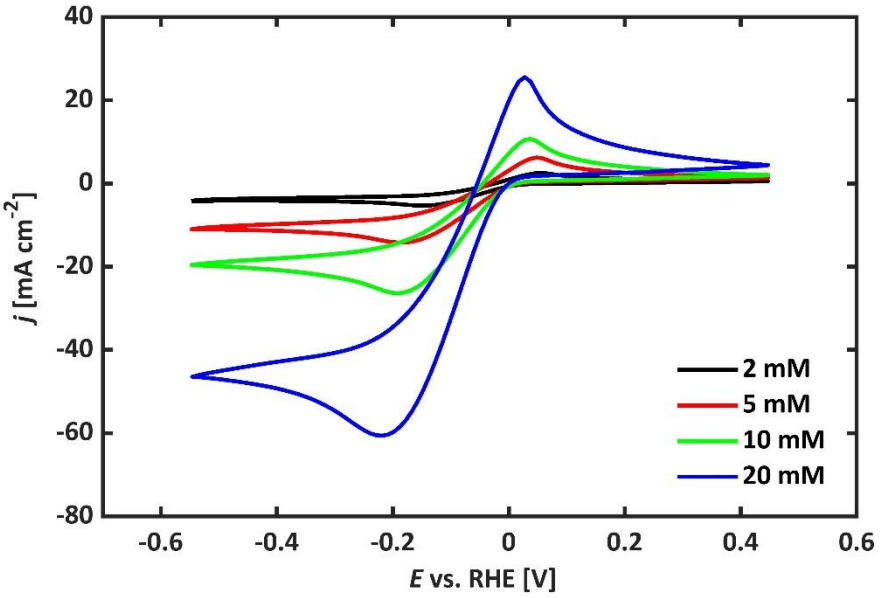
40
20
0
-20
-40
-60
-80
-0.6
-0.4
-0.2
0
0.2
0.4
0.6
j [mA cm-2]
E vs. RHE [V]
2 mM
5 mM
10 mM
20 mM

Figure 2

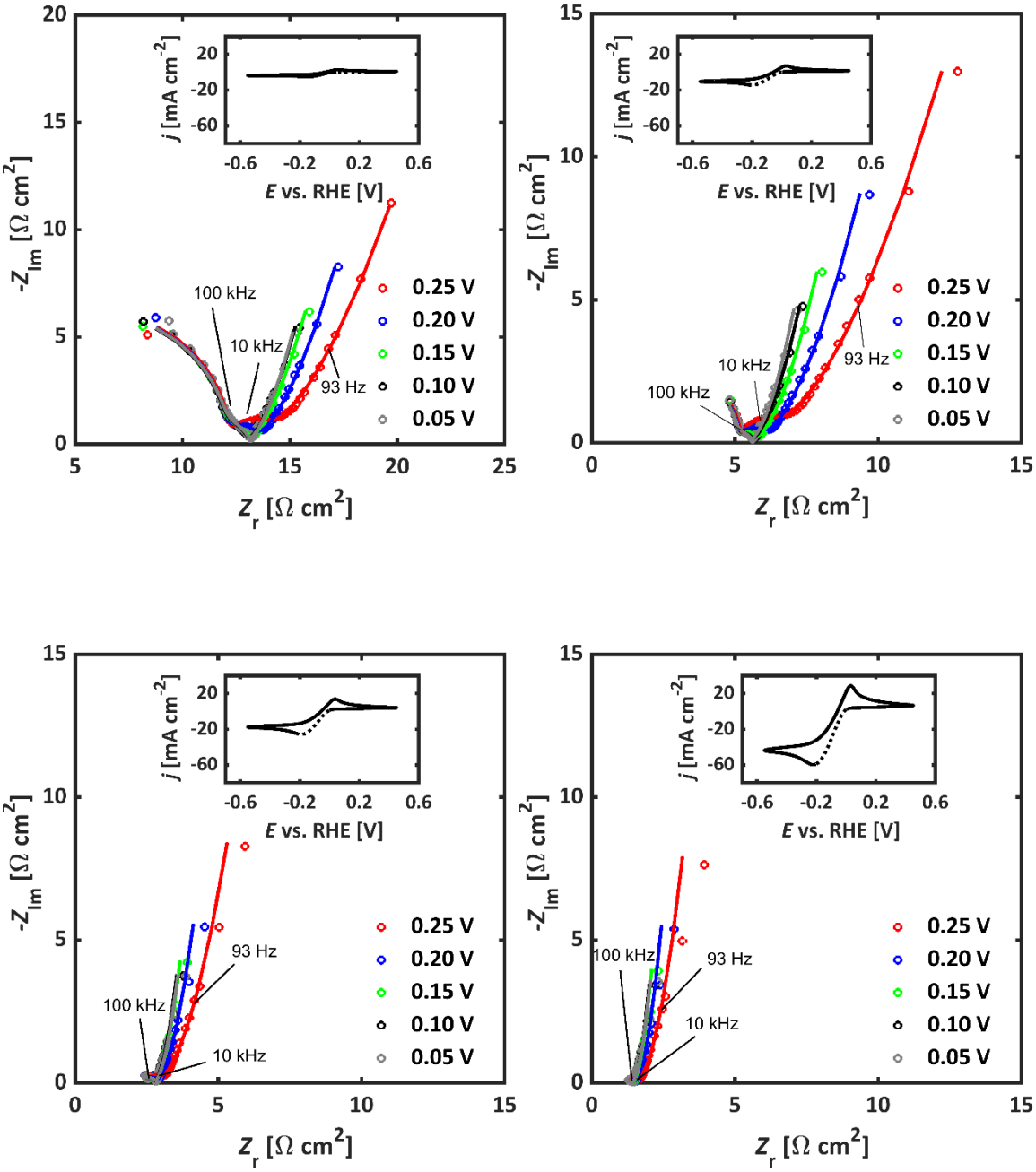
-Z_Im [Ω cm^2]
Z_r [Ω cm^2]
j [mA cm^-2]
E vs. RHE [V]
100 kHz
10 kHz
93 Hz
0.25 V
0.20 V
0.15 V
0.10 V
0.05 V

Figure 3

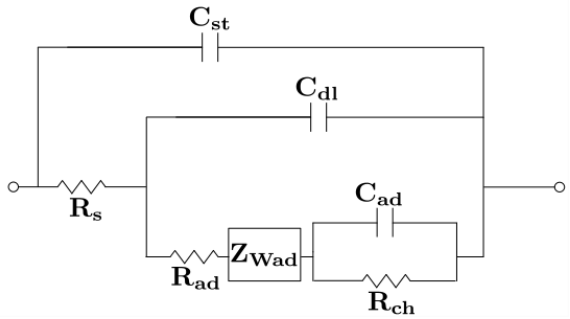

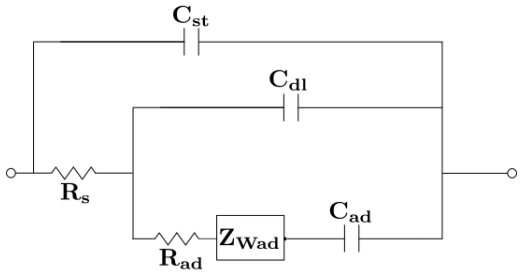

Figure 4

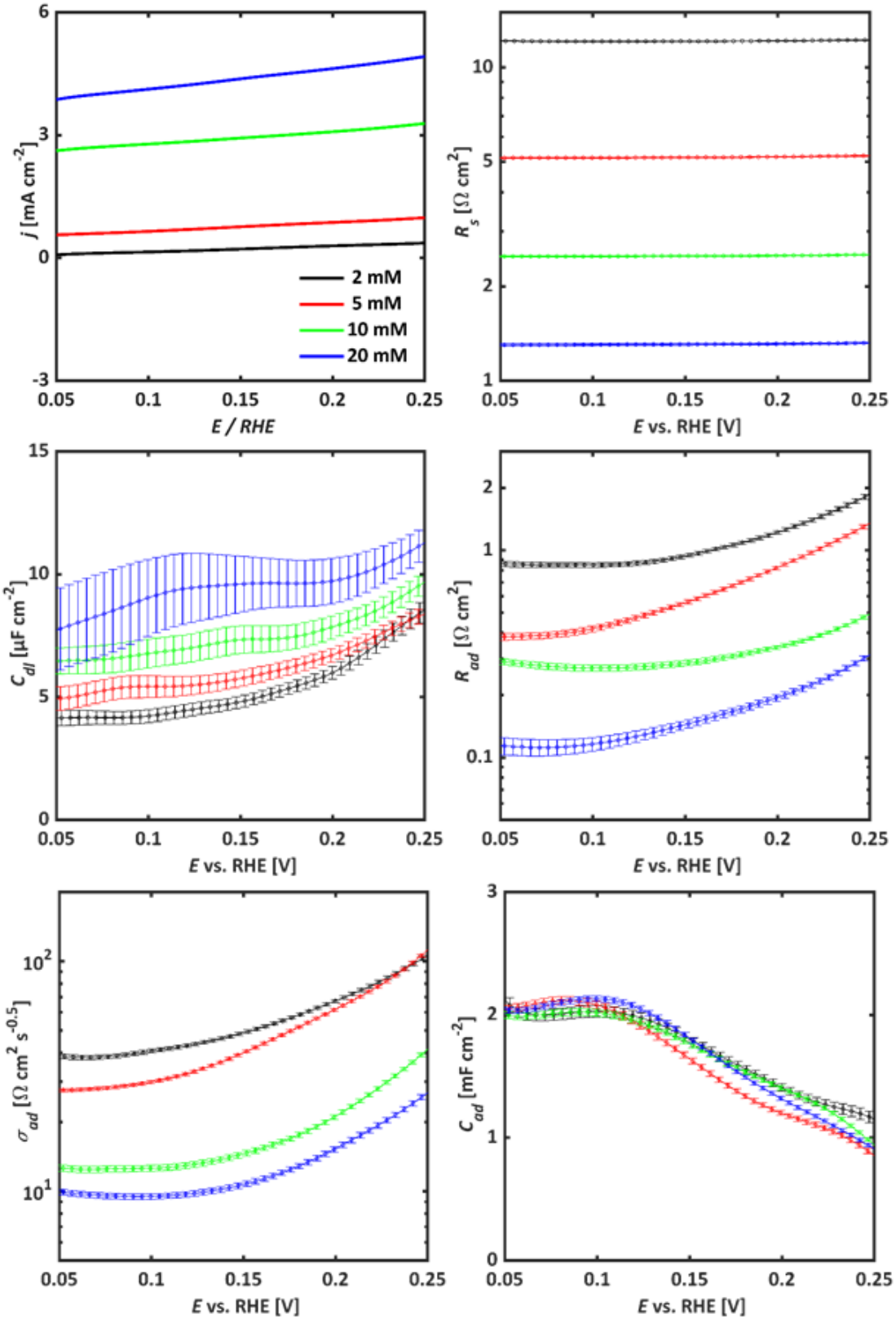
j [mA cm-2]
E / RHE
2 mM
5 mM
10 mM
20 mM
Rs [Ω cm2]
E vs. RHE [V]
Cdl [μF cm-2]
E vs. RHE [V]
Rad [Ω cm2]
E vs. RHE [V]
σad [Ω cm2 s-0.5]
E vs. RHE [V]
Cad [mF cm-2]
E vs. RHE [V]

Figure 5

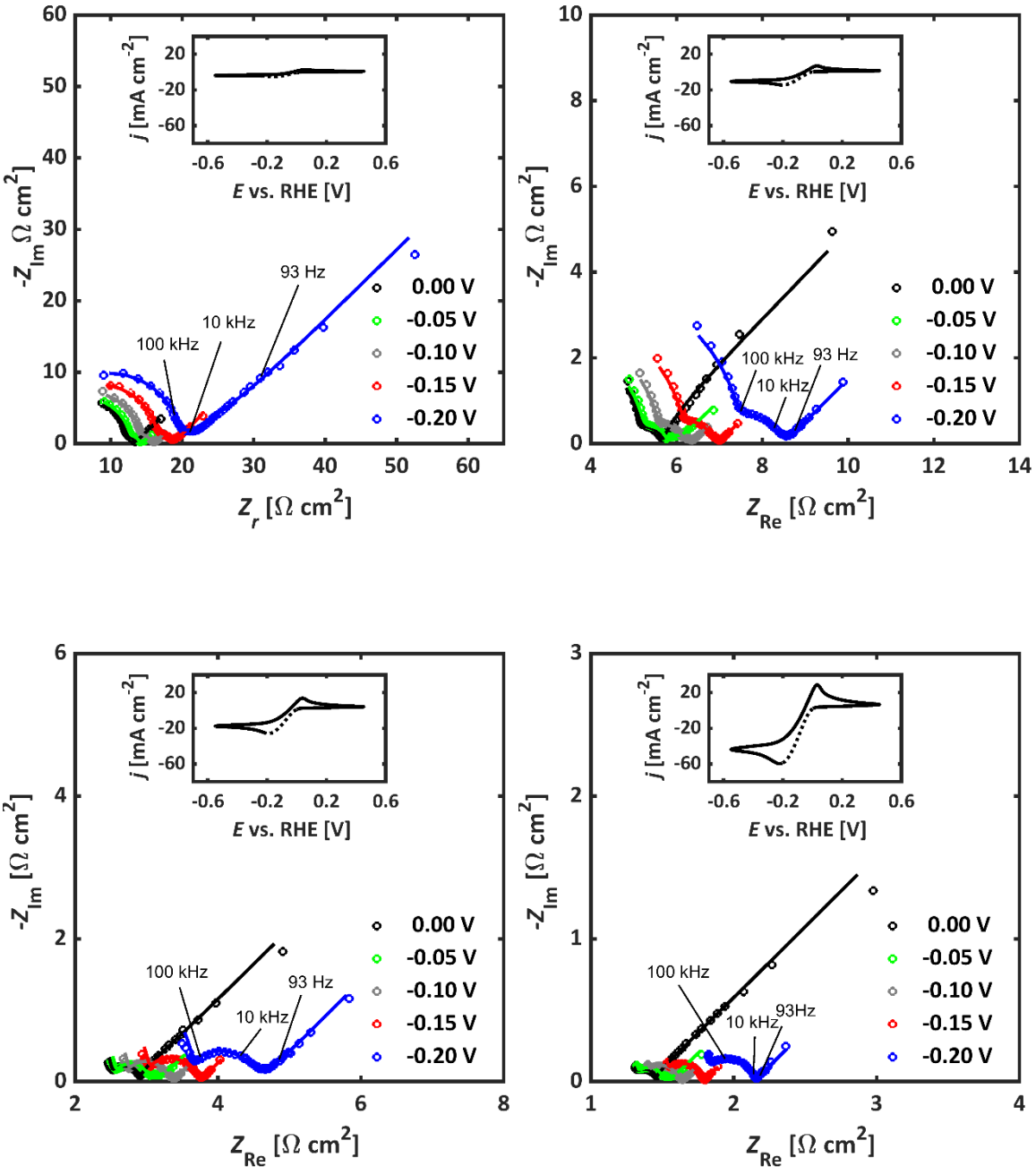
-Z_Im Ω cm^2
Z_r [Ω cm^2]
Z_Re [Ω cm^2]
j [mA cm^-2]
E vs. RHE [V]
100 kHz
10 kHz
93 Hz
93Hz
0.00 V
-0.05 V
-0.10 V
-0.15 V
-0.20 V

Figure 6

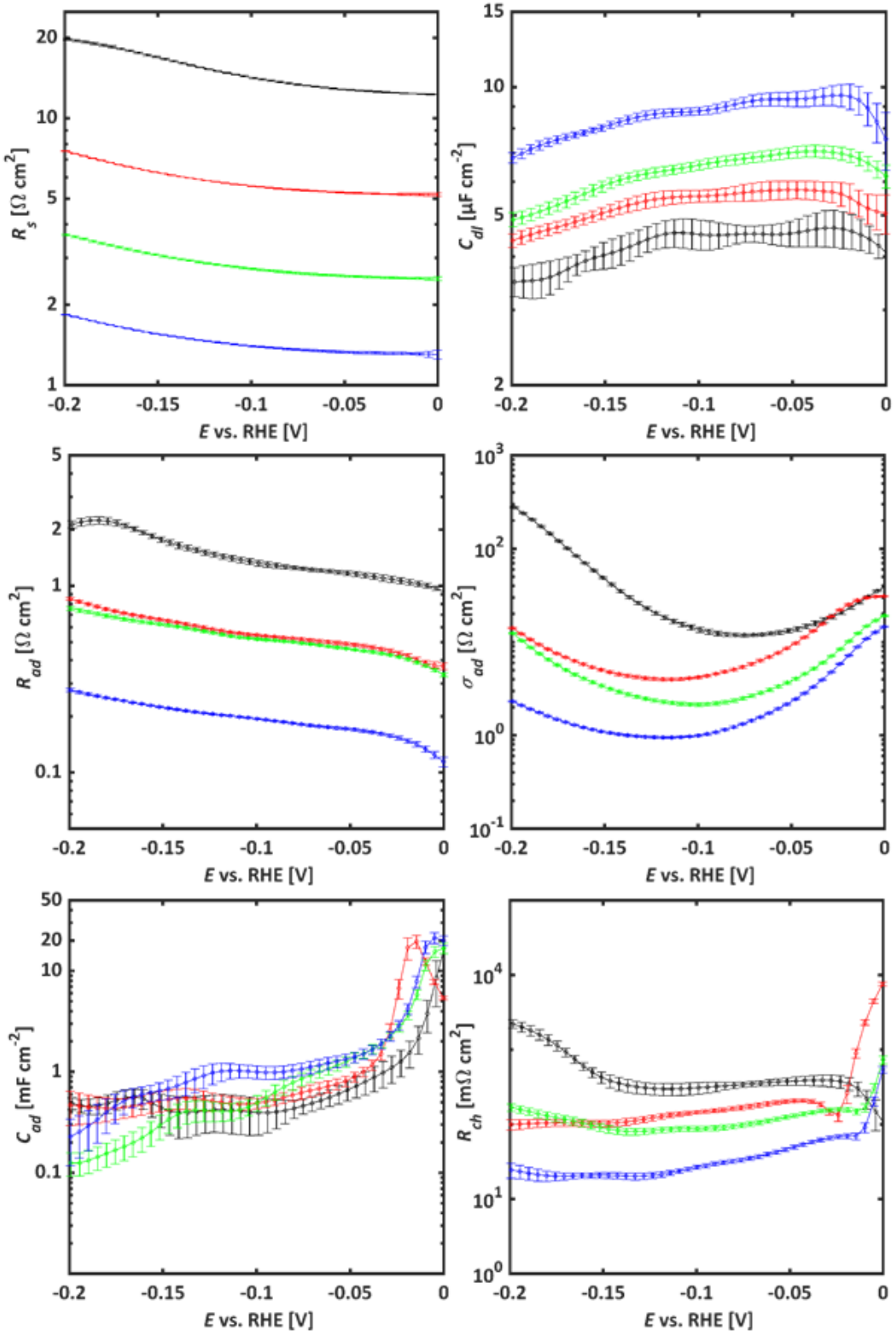
R_s [Ω cm^2]
C_{dl} [µF cm^{-2}]
R_{ad} [Ω cm^2]
σ_{ad} [Ω cm^2]
C_{ad} [mF cm^{-2}]
R_{ch} [mΩ cm^2]
E vs. RHE [V]

Table 1

$c(HClO_4)$ [mM]	$R_{s\,cal}$ [Ω cm^2]	$R_{s\,fit}$ [Ω cm^2]
2	11.8	12.1
5	4.71	5.15
10	2.35	2.51
20	1.17	1.31

Table 2

$c(HClO_4)$ [mM]	τ_{st} [ns]	f_{st} [MHz]	τ_{ad} [µs]	f_{ad} [kHz]
2	120	1.30	4.10	39.0
5	53.0	3.00	3.10	51.0
10	26.0	6.20	2.20	74.0
20	13.0	12.0	1.30	120

Table 3

$c(HClO_4)$ [mM]	τ_{ad} [µs]	f_{ad} [kHz]	τ_{ch} [µs]	f_{ch} [kHz]
2	5.30	30.0	50.0	2.88
5	2.70	60.0	40.0	3.59
10	3.70	43.0	30.0	4.36
20	1.70	93.0	18.8	8.45